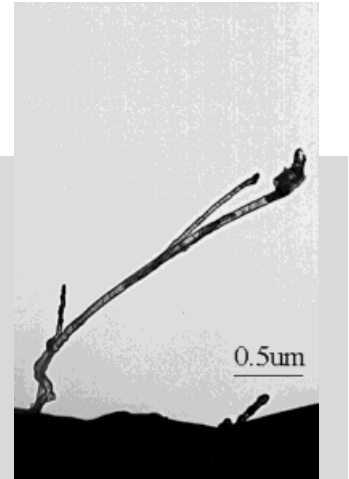


Nano-Scale Mechanics of Nanotubes, Nanowires, and Nanobelts**

By Zhong L. Wang,* Rui Ping Gao, Zheng Wei Pan, and Zu Rong Dai

One-dimensional (1D) nanostructures have numerous potential applications in science and engineering. Nanocomposites made of nanowires, such as carbon nanotubes, are likely to decrease material's density and increase its strength,^[1] which are of critical importance to space technology. To investigate the uniqueness offered by these materials, new techniques must be developed to quantitatively measure the properties of individual wire-like structures whose structures are well characterized by electron microscopy techniques, because their properties may sensitively depend on their geometrical shape/configurations and crystal as well as surface structures. Within the framework of in-situ TEM we have recently developed a novel approach that relies on electric field induced mechanical resonance for measuring the properties of individual wire-like structures, such as Young's modulus, electron field emission, tip work function, and electrical quantum conductance. This is a new technique that provides the properties of a single nanowire with well characterized.



1. Introduction

One-dimensional (1D) nanostructures have numerous potential applications in science and engineering. Nanocomposites made of nanowires, such as carbon nanotubes, are likely to decrease material's density and increase its strength,^[1] which are of critical importance to space technology. Nanowires may serve as the interconnects and devices for nanoelectronics and optoelectronics.^[2] Searching for interconnects is the key for quantum devices and nano-scale system integration. Aligned nanowires have exceptional field emission properties,^[3] such as low operation voltage, high efficiency and high brightness. Semiconductor nanowires are the fundamental components for nano-scale device fabrication based on the concept of building devices using a single wire.

In geometrical structures, the 1D nanostructures can be classified into five main groups: 1) hollow nanotubes,^[4] 2) solid nanowires,^[5-7] 3) coaxial cable structures,^[8] 4) side-by-side biaxial nanowires,^[9] structured by stacking of two nanowires of different materials in parallel; and 5) nanobelts (or nanoribbons),^[10] which have a rectangular cross-section, in correspondence to a belt-like morphology. The first three have a common characteristic of cylindrical symmetric cross-section. The distinctive geometrical shapes of these 1D nanostructures

are likely to be important in determination of their mechanical, electrical, optical, and thermal transport properties. To investigate the uniqueness offered by these shapes, new techniques must be developed to quantitatively measure the properties of individual wire-like structures whose structures are well characterized by electron microscopy techniques,

[*] Prof. Z. L. Wang, Dr. R. P. Gao, Dr. Z. W. Pan, Dr. Z. R. Dai
Center for Nanoscience and Nanotechnology
School of Materials Science and Engineering
Georgia Institute of Technology
Atlanta, GA 30332-0245 (USA)
E-mail: zhong.wang@mse.gatech.edu

[**] Thanks the support from NSF grants DMR-9733160, the NSF of China, and the Georgia Tech Electron Microscopy Center. We are grateful to Professor W.A. de Heer, Dr. P. Poncharal, Professor J. L. Gole, Dr. Liming Dai, Dr. M. Gao, Mr. J. D. Stout for the collaboration toward the work reviewed in this article.

Thanks to the financial support of US NSF grants DMR-9971412 and DMR-9733160 and the NSF of China, the Georgia Tech Electron Microscopy Center for providing the research facility, and Dr. J. Bradley for kind help in specimen preparation.

because their properties may sensitively depend on their geometrical shape/configurations and crystal as well as surface structures.

Scanning probe microscopy (scanning tunneling microscopy, STM, atomic force microscopy, AFM) has been a powerful tool in manipulating and characterizing the properties of individual nanostructures. Thus far, this technique has provided the dominant approach to nano-scale manipulation.^[10,11] Transmission electron microscopy (TEM), on the other hand, has been traditionally applied to the characterization of the intrinsic structures of nanomaterials. The measurement of the Young's modulus of carbon nanotubes was first carried out using TEM by quantifying the thermal vibration amplitude of the nanotube.^[12] Within the framework of in-situ TEM we have recently developed a novel approach that relies on electric field induced mechanical resonance for measuring the properties of individual wire-like structures, such as Young's modulus,^[13] electron field emission,^[14] tip work function,^[15] and electrical quantum conductance.^[16] This is a new technique that provides the properties of a single nanowire with well characterized. In this paper, we present a brief review on our recent progress in characterizing the nano-scale mechanical properties of wire-like structures using in-situ TEM.

2. Bending Modulus of Nanowire Objects

To correlate the measured mechanical property with the intrinsic microstructure of a nanowire, our measurements were made in-situ in a TEM, through which the morphology, defect structure and real dimensions of the object are unambiguously determined.^[17] The specimen holder requires the translation of the nanowire via either mechanical movement by a micrometer or axial directional piezo (Fig. 1a). The static and dynamic properties of the nanowires can be obtained by applying a controllable static and alternating electric field. The nanowires were glued using silver past onto a gold wire, through which the electric contact was made. The counter electrode is a solid Au ball. An electric field can be applied across the two electrodes for inducing mechanical resonance. The nanowire to be used for property measurements is directly imaged under TEM (Fig. 1b), and electron diffraction patterns and images can be recorded from the nanowire, which directly gives the morphological and structural information of the nanowire. The distance from the nanowire to the counter electrode is controllable.

Our experiments were carried out using an JEOL 100C TEM (100 kV), which has the advantage of large angle specimen tilt and negligible radiation damage. An oscillating voltage with tunable frequency was applied on the nanowires. Mechanical resonance can be induced in the nanowire if the applied frequency approaches the resonance frequency (Fig. 1c). We have previously showed that the classical continuous medium theory can still be applied to determine the resonance behavior of a solid beam with diameters of a few tens of nanometers.

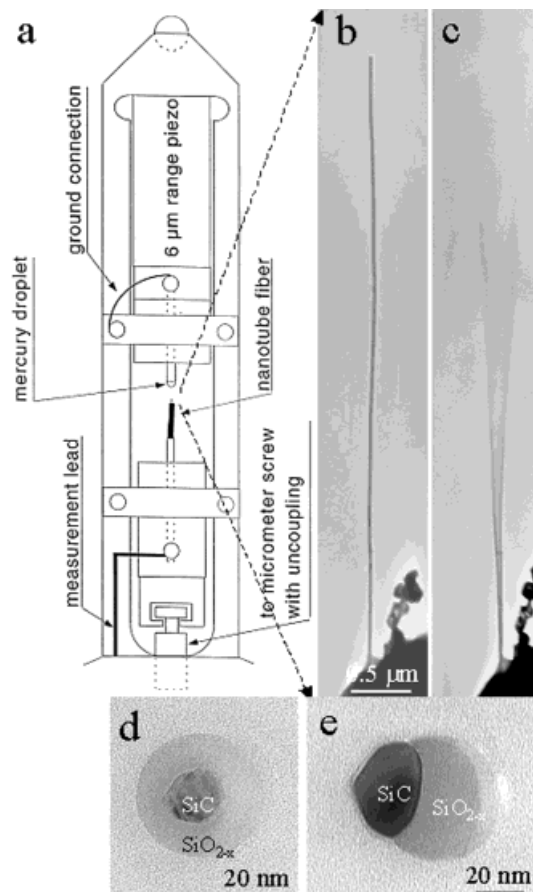


Fig. 1. a) Schematics of the TEM specimen holder for the in-situ measurements. b), c) A silica sheathed crystalline silicon nanowire at stationary and the first harmonic resonance induced by an externally applied electric field, respectively. The applied alternating current (AC) voltage was 10 V and the resonance frequency was 693 kHz. d), e) Cross-sectional TEM images of coaxially structured SiC-SiO_{2x} and biaxially structured SiC-SiO_{2x} nanowires, respectively.

For a beam with one end hinged and the other free, the resonance frequency is given by:

$$f_0 = (\beta^2 / 2\pi)(EI/m)^{1/2} / L^2 \quad (1)$$

where f_0 is the fundamental resonance frequency, $\beta = 1.875$, EI is the flexural rigidity (or bending stiffness), E is the Young's modulus, I is the moment of inertia about a particular axis of the rod, L is the length of the beam, and m is its mass per unit length. If the geometrical shape of the nanowire is known from cross-sectional TEM images (Figs. 1d and e), its moment of inertia can be calculated using the standard definition in mechanics, thus, Equation 1 can be applied to the cases of carbon nanotubes, coaxial and biaxial nanowires, as long the true fundamental frequency is identified.^[17]

Our first group of experiments was carried out for carbon nanotubes produced by an arc-discharge technique, which are believed to be free from defects. The carbon nanotubes have diameters 5–50 nm and lengths of 1–20 μm and most of them are nearly defect-free. After a systematic studies of the multi-walled carbon nanotubes, the bending moduli of the nanotubes were measured as a function of their diameters.^[13]

The bending modulus is as high as 1.2 TPa (as strong as diamond) for nanotubes with diameters smaller than 8 nm, and it drops to as low as 0.2 TPa for those with diameters larger than 30 nm. A decrease in bending modulus as the increase of the tube diameter is attributed to the wrinkling effect of the wall of the nanotube during small bending. This effect almost vanishes when the diameters of the tubes are less than 12 nm.

Carbon nanotubes produced by pyrolysis usually contain a high density of defects owing to the introduction of pentagonal and heptagonal carbon-rings. To quantitatively determine the effect of growth defects on the bending modulus of carbon nanotubes, the mechanical properties of the aligned carbon nanotubes prepared by pyrolysis of iron(II) phthalocyanine were used.^[18] The carbon nanotubes display the bamboo-like structure, which is very different from those produced by arc-discharge. If the structure of the carbon nanotubes can be approximated as a uniform tube structure, the bending modulus of the tube can be calculated using Equation 1 from the experimentally measured resonance frequency. The bending modulus of nanotubes with point defects was ~30 GPa. For nanotubes with a visible volume defect along its length, such as the node or a collapsed wall, their modulus was 2–3 GPa, almost 10–15 times smaller than that of the nanotubes without the volume defects in the same group of sample. It is apparent that the bending modulus is much lower than those for the nanotubes of equivalent sizes produced by arc-discharge.

To trace the effect of a volume defect on the mechanical properties, we have examined the electrostatic deflection of a nanotube when a constant voltage is applied across the electrodes (Fig. 2). The nanotube shows a smooth deflection without visible change in its shape near the volume defect. We did not observe an abrupt change in the nanotube shape at a defect point. Therefore, the volume defect seems do not introduce any significant softening at the local region, due, most probably, to the collectively rippling deformation on the inner arc of the bent nanotube.^[13] The in-situ TEM provides a powerful approach towards nanomechanics of fiber-like nanomaterials with well characterized defect structures.

Testing the creeping property of nanomaterials is a challenge. The technique we developed may be applied for such a purpose although we still cannot perform the experiments at higher temperatures. Figure 3 shows the mechanical resonance of a carbon nanotube at extremely large vibration amplitude. The total vibrations were for more than 10^9 cycles during one hour of resonance, and the structure is still intact. The nanotube remains elastic after the large dynamic bending.

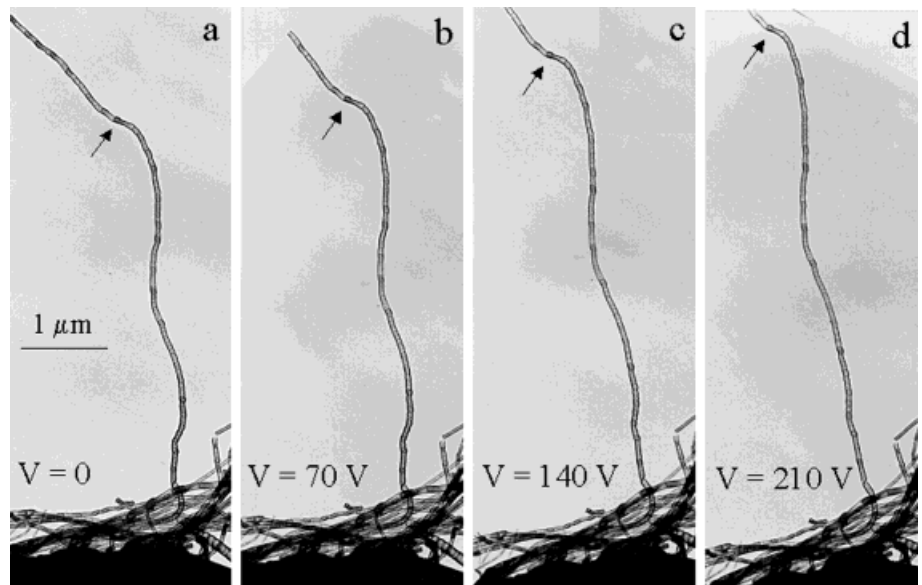


Fig. 2. Electrostatic deflections of a carbon nanotube under the applied direct current (DC) voltage, showing no local softening at the site of a volume defects as indicated by an arrowhead.

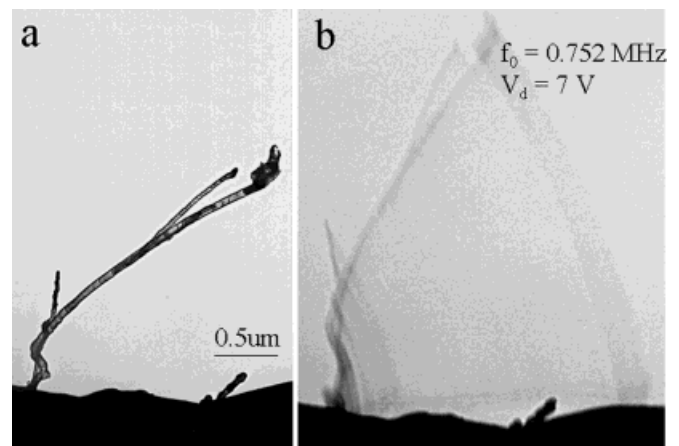


Fig. 3. A carbon nanotube at a) stationary and b) mechanical resonance ($f_0 = 0.752$ MHz), showing the possibility of performing room temperature creep testing of a nanowire object.

3. Young's Modulus of Nanowires

We have recently synthesized composite nanowires, such as coaxial silicon nanowires sheathed by a thin layer of SiO_2 and the biaxial SiC-SiO_x nanowires that consist of two side-by-side sub-nanowires of silica and $\beta\text{-SiC}$.^[9] The $\beta\text{-SiC}$ portion of the nanowires usually has a higher density of stacking faults and twins, which are important for the formed shape and structure of the nanowires. The density of the planar defects determines the growth direction of the nanowires. A high density of planar defects results in a $[311]$ axial direction for the biaxial nanowires, in contrast to $[111]$ for the coaxial nanowires. Biaxial nanowires with a much lower density of stacking faults has the $[211]$ growth direction.

The Young's modulus of the composite nanowires was measured for pure silica nanowires (Table 1). It can be seen

Table 1. Measured Young's modulus, E , for solid silica nanowires. E was calculated using the density of bulk amorphous SiO_2 . f_0 : the fundamental resonance frequency; L : nanowire length; D : nanowire diameter.

D [nm] (2 nm)	L [μm] ($\pm 0.2 \mu\text{m}$)	f_0 [MHz]	E [GPa]
42	11.7	0.160	31 ± 5.1
53	6.3	0.562	20 ± 4.0
58	3.8	1.950	27 ± 7.5
70	13.0	0.200	26 ± 3.1
95	14.8	0.232	32 ± 3.1

that the data are fairly consistent, and we obtain a Young's modulus about half of that for large size silica fibers. For a coaxial cable structured nanowire whose core material density is ρ_c and diameter is D_c and a sheath material density, which is ρ_s with outer diameter D_s , the average density of the nanowire is given by

$$\rho_e = \rho_c(D_c^2/D_s^2) + \rho_s(1 - D_c^2/D_s^2) \quad (2)$$

The effective Young's modulus of the composite nanowire, E_{eff} , is given by

$$E_{\text{eff}} = \rho_e[8\pi f_0 L^2 / \beta^2 D_s^2] \quad (3)$$

The bending modulus for the coaxial cable structured SiC-SiO_x nanowires results in combination from SiC and SiO_x, where the contribution from the sheath layer of SiO_x is more weighted than that from the SiC core because of its larger flexural rigidity (or bending stiffness) (see Fig. 1d). The bending modulus increases as the diameter of the nanowire increases (Table 2). The measured Young's modulus can be compared with the theoretically predicted values based on the effective flexural rigidity of a composite coaxial nanowire, which is $E_{\text{eff}}I_{\text{eff}} = E_{\text{SiC}}I_{\text{SiC}} + E_{\text{SiO}_x}I_{\text{SiO}_x}$, where the values for the bulks are $E_{\text{SiC}} = 466$ GPa and $E_{\text{SiO}_x} = 73$ GPa. Thus, the effective Young's modulus of the nanowire with cylindrical symmetry is given by $E_{\text{eff}} = \alpha E_{\text{SiC}} + (1 - \alpha)E_{\text{SiO}_x}$, where $\alpha = (D_c/D_s)^4$. The calculated value agrees well with the measured value on the trend of the modulus as a function of their diameters, but the theory seems overestimate the modulus.

Table 2. Measured Young's modulus of coaxial cable structured SiC-SiO_x nanowires (SiC is the core, and silica is the sheath). The densities of SiC and SiO₂ were taken from the bulk values ($\rho_{\text{SiC}} = 2.2 \times 10^3$ kg/m³; $\rho_{\text{SiO}_2} = 3.2 \times 10^3$ kg/m³). D_s and D_c are the outer and inner diameters of the SiO_x sheath, respectively.

D_s [nm] (± 2 nm)	D_c [nm] (± 1 nm)	L [μm] (0.2 μm)	f_0 [MHz]	E_{eff} [GPa] Exp.	E_{eff} [GPa] Theo.
51	12.5	6.8	0.693	46 ± 9.0	73
74	26	7.3	0.953	56 ± 9.2	78
83	33	7.2	1.044	52 ± 8.2	82
132	48	13.5	0.588	78 ± 7.0	79
190	105	19.0	0.419	81 ± 5.1	109

The Young's modulus of a biaxial nanowire can be calculated analogously, except that the moment of inertial must be calculated with consideration the cross-sectional geometry of the nanowire, as shown in Figure 1e. The results are summarized in Table 3 and detailed calculation has been given elsewhere.

Table 3. Measured Young's modulus of biaxially structured SiC-SiO_x nanowires. D_{wire} and D_{SiC} are the widths across the entire nanowire and across the SiC sub-nanowire, respectively.

D_{wire} [nm] (± 2 nm)	D_{SiC} [nm] (± 1 nm)	L [μm] (± 0.2 m)	f_0 [MHz]	E_{eff} [GPa] Exp.
58	24	4.3	1.833	54 ± 24.1
70	36	7.9	0.629	53 ± 8.4
83	41	4.3	2.707	61 ± 13.8
92	47	5.7	1.750	64 ± 14.3

The tensile strengths of individual carbon nanotubes have been measured by Yu et al.^[19] with a nanostressing stage located within a scanning electron microscope (SEM). A carbon nanotubes was glued at both ends to two AFM tips facing each other, and the tensile-loading experiment was prepared and observed entirely within the microscope and was recorded on video. The nanotube broke in the outermost layer and the tensile strength of this layer ranged from 11 to 63 GPa. Analysis of the stress-strain curves for individual nanotube indicated that the Young's modulus of the outermost layer varied from 270 to 950 GPa.

4. Semiconductive Oxide Nanobelts

Using thermal evaporation of oxide powders under controlled conditions, we have recently synthesized nanobelt structures of ZnO, SnO₂, In₂O₃, CdO, Ga₂O₃, and PbO₂.^[20] The as-synthesized oxide nanobelts are pure, structurally uniform, single crystalline and most of them free from defects and dislocations; they have a rectangular-like cross-section with typical an average width of ~200 nm, width-to-thickness ratios of 5-10 and lengths of up to a few millimeters. Figure 4a gives a SEM image of the as-synthesized In₂O₃ nanobelts, and a corresponding TEM image is given in Figure 4b. Each nanobelt is a single crystal without the presence of dislocations; its morphology and structure, such as growth direction and surface planes, are well defined, and their surfaces are clean and atomic flat. In contrast to conventional bulk ceramics, the nanobelt is highly flexible and it can be bend for >90° at half without breaking.

The belt-like morphology appears to be a unique and common structural characteristic for the family of semiconductive oxides with cations of different valence states and materials of distinct crystallographic structures. Their structures are well controlled, and the belt shape is defined by some specific crystallographic planes. Table 4 gives a summary on the growth directions and the surface planes of the nanobelts of

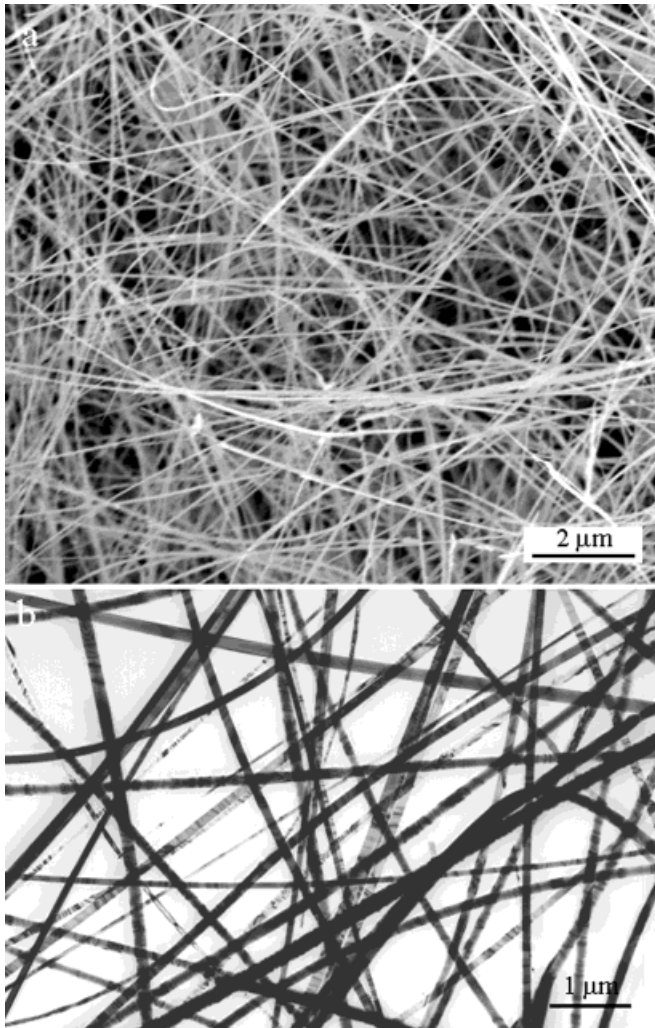


Fig. 4. a) SEM image of the as-synthesized In_2O_3 nanobelts. b) TEM image of the nanobelts.

Table 4. Semiconductive oxide nanobelts and their growth directions and surface planes.

Nanobelts	Crystal structure	Growth direction in plane	Top Surface	Side surfaces
ZnO	Wurtzite	[0001]	$\pm (2\bar{1}\bar{1}0)$	$\pm (0\bar{1}\bar{1}0)$
ZnO	Wurtzite	[01 $\bar{1}0$] [a]	$\pm (2\bar{1}\bar{1}0)$	$\pm (0001)$
Ga ₂ O ₃	Monoclinic	[10 $\bar{1}$]	$\pm (10\bar{1})$	$\pm (010)$
Ga ₂ O ₃	Monoclinic	[010]	$\pm (010)$	$\pm (10\bar{1})$
SnO ₂	Rutile	[101]	$\pm (10\bar{1})$	$\pm (010)$
In ₂ O ₃	C-Rare earth	[001]	$\pm (100)$	$\pm (010)$
CdO	NaCl	[001]	$\pm (100)$	$\pm (010)$
PbO ₂	Rutile	[100]	$\pm (001)$	$\pm (010)$

[a] The nanobelts have a single stacking fault/twin parallel to the growth direction throughout the entire length.

different materials that we have successfully synthesized. The semiconductive oxide nanobelts could be used for fabrication of nano-scale electronic and optoelectronic devices. With a well-defined geometry and perfect crystal structure, the nanobelts are likely to be a model materials family for a systematic understanding in the electrical, thermal, optical and ionic transport processes as well as mechanical behavior in quasi-1D nanostructures with the absence of dislocations. This will be an exciting new field for nanomaterials.

[1] P. M. Ajayan, P. Redlich, M. Ruhle, *J. Microsc.* **1997**, 185, 275.

[2] X. F. Duan, Y. Huang, Y. Cui, J. Wang, C. M. Lieber, *Nature* **2001**, 409, 66.

[3] W. A. De Heer, A. Chatelain, D. Ugarte, *Science* **1995**, 268, 845.

[4] S. Iijima, *Nature* **1991**, 354, 56.

[5] A. M. Morales, C. M. Lieber, *Science* **1998**, 279, 208.

[6] S. T. Lee, N. Wang, Y. F. Zhang, Y. H. Tang, *MRS Bull.* **1999**, August, 36.

[7] D. P. Yu, Z. G. Bai, Y. Ding, Q. L. Hang, H. Z. Zhang, J. J. Wang, Y. H. Zou, W. Qian, G. C. Xiong, H. T. Zhou, S. Q. Feng, *Appl. Phys. Lett.* **1998**, 72, 3458.

[8] Y. Zhang, K. Suenaga, C. Colliex, S. Iijima, *Science* **1998**, 281, 973.

[9] Z. L. Wang, Z. R. Dai, Z. G. Bai, R. P. Gao, J. Gole, *Appl. Phys. Lett.* **2000**, 77, 3349.

[10] E. Wong, P. Sheehan, C. Lieber, *Science* **1997**, 277, 1971.

[11] J. P. Salvetat, A. J. Kulik, J. M. Bonard, G. A. D. Briggs, T. Stockli, K. Metenier, S. Bonnamy, F. Beguin, N. A. Burnham, L. Forro, *Adv. Mater.* **1999**, 11, 161.

[12] M. M. Treacy, T. W. Ebbesen, J. M. Gibson, *Nature* **1996**, 38, 678.

[13] P. Poncharal, Z. L. Wang, D. Ugarte, W. A. de Heer, *Science* **1999**, 283, 1516.

[14] Z. L. Wang, P. Poncharal, W. A. de Heer, *Microsc. Microanal.* **2000**, 6, 224.

[15] R. P. Gao, Z. L. Wang, Z. W. Pan, *Appl. Phys. Lett.* **2001**, 78, 1757.

[16] S. Frank, P. Poncharal, Z. L. Wang, W. A. de Heer, *Science* **1998**, 280, 1744.

[17] Z. L. Wang, P. Poncharal, W. A. De Heer, *Pure Appl. Chem.* **2000**, 72, 209.

[18] S. M. Huang, L. M. Dai, A. W. H. Mau, *J. Phys. Chem. B* **1999**, 103, 4223.

[19] M. F. Yu, O. Lourie, M. J. Dyer, K. Moloni, T. F. Kelly, R. S. Ruoff, *Science* **2000**, 287, 637.

[20] Z. W. Pan, Z. R. Dai, Z. L. Wang, *Science* **2001**, 291, 1947.